Treatment of Layered Structures Using a Semilocal meta-GGA Density Functional

ARTICLE *in* JOURNAL OF PHYSICAL CHEMISTRY LETTERS · DECEMBER 2009

Impact Factor: 7.46 · DOI: 10.1021/jz9002422

3 AUTHORS, INCLUDING:

Georg K. H. Madsen
Ruhr-Universität Bochum
92 PUBLICATIONS **6,980** CITATIONS

THE JOURNAL OF PHYSICAL CHEMISTRY Letters

pubs.acs.org/JPCL

Treatment of Layered Structures Using a Semilocal meta-GGA Density Functional

Georg K. H. Madsen,*[,†,‡] Lara Ferrighi,[†] and Bjørk Hammer[‡]

[†]ICAMS, Ruhr Universität Bochum, Germany and [‡]Interdisciplinary Nanoscience Center (iNANO) and Department of Physics and Astronomy, Aarhus University, DK-8000 Aarhus C, Denmark

ABSTRACT Density functional theory calculations on solids consisting of covalently bonded layers held together by dispersive interactions are presented. Utilizing the kinetic energy density in addition to the density and its gradients gives the meta-generalized gradient approximation (MGGA) M06-L enough flexibility to treat correctly both the covalent and the dispersive interactions in layered solids, thus making it a significant step forward compared to the local density and generalized gradient approximations. We show how the MGGA can take advantage of the extra information in the kinetic energy density to discriminate between dispersive and covalent interactions and thereby prove that the performance of M06-L for dispersive interactions, as opposed to that for the local density approximation, is not based on an accidental cancellation of errors.

SECTION Electron Transport, Optical and Electronic Devices, Hard Matter

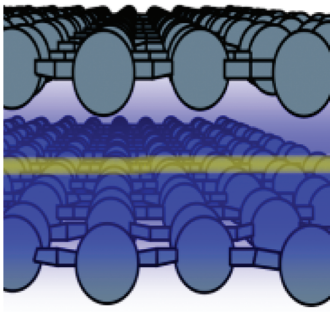

Weak dispersive interactions play an important role in the behavior of large biomolecules, soft matter, supermolecular chemistry, materials, and catalysts. While density functional theory (DFT) in its generalized gradient approximation (GGA) has become a preferred modeling tool, it is conventional wisdom that GGAs have problems describing dispersive interactions. This can be seen, for example, in graphite, where the *c*-axis is overestimated by almost 40%.[1] Some authors have resorted to using the local density approximation (LDA) for dispersively bonded systems since it accidentally gives good results. This approach is, of course, unsatisfactory since it restores the strong overbinding of covalent bonds, a problem otherwise solved by the GGA. One solution has been to remedy the GGA problem by empirical corrections to the energy.[2−4] However, there is an obvious interest in a more general treatment of dispersive interactions within DFT. Several approaches have recently been developed, ranging from modeling the dipole moment of the exchange hole[5] to a fully nonlocal correlation functional.[6]

The successes of these treatments of dispersive interactions as add-ons to a plain DFT description come at the expense of complexity. None of them have a (semi)local exchange correlation energy, which otherwise is both a conceptual and practical advantage of DFT. This is, however, offered by the meta-generalized gradient approximation (MGGA), which includes the kinetic energy density in addition to the electron density and its gradients in the functional expression. In this Letter, we will focus on the M06-L-MGGA functional by Zhao and Truhlar.[7] The M06-L was constructed by fitting a functional form with 25 parameters to a large database of organic and organometallic compounds. Interestingly, the database included interactions such as the $\pi-\pi$ bond between two benzene rings. We will in the present work analyze the performance of the M06-L with respect to dispersive interactions, focusing on what we see as the three major points.

First, we demonstrate that the M06-L has enough flexibility to treat correctly both the covalent and the dispersive interactions in layered solids, thus making it a significant step forward compared to the LDA and GGAs. Second, our test systems are graphite, hexagonal boron nitride (*h*-BN), and molybdenum disulfite (MoS_2). While the first is related to benzene, the two other systems lie well outside of the compounds represented in the database used to parametrize M06-L. Thereby, the robustness of the functional, an obvious concern when using a fitted functional, is tested. Furthermore we will use the elastic constants to probe the second derivatives of the energy surface. Finally, we prove that the performance of M06-L on dispersive interactions, as opposed to the LDA, is not based on an accidental cancellation of errors. We show how the MGGA can take advantage of the extra information in the kinetic energy density to discriminate between dispersive and covalent interactions. The calculations were carried out using the GPAW (grid-based projector-augmented wave) code.[8] The details of the calculation are reported in the Supporting Information. The bulk modulus, B_0, was derived from the elastic constants as

$$B_0 = \frac{C_{33}(C_{11}+C_{12})-2C_{13}^2}{(C_{11}+C_{12})+2C_{33}-4C_{13}} \quad (1)$$

Table 1 provides the lattice constants and cohesive energies of the three systems. The LDA gives a good prediction of the lattice constants but strongly overestimates the cohesive

Received Date: November 9, 2009
Accepted Date: December 17, 2009
Published on Web Date: December 28, 2009

DOI: 10.1021/jz9002422 | *J. Phys. Chem. Lett.* **2010**, *1*, 515–519

Table 1. Structural Properties of Graphite, *h*-BN, and MoS_2[a]

	graphite				*h*-BN				MoS_2			
	LDA	PBE	M06-L	exp	LDA	PBE	M06-L	exp	LDA	PBE	M06-L	exp
a_0	2.446	2.468	2.451	2.462	2.490	2.514	2.500	2.504	3.138	3.190	3.164	3.16
c_0	6.620	9.166	6.719	6.707	6.504	8.613	6.670	6.660	12.10	16.400	12.61	12.29
E_c	8.9	7.9	7.7	7.42[9]	16.0	14.0	13.6	13[10]	18.7	15.0	15.3	15.0[9]
E_l	25	< 1	41	35(15)[11] 52(5)[12]								

[a] The lattice constants are in Å. The cohesive energy and the interlayer cohesive energy are in eV per formula unit and meV per formula unit, respectively. The experimental cohesive energy for *h*-BN is taken from the footnote of Table 2 in ref 10.

Table 2. Elastic Properties of Graphite, *h*-BN, and MoS_2 in GPa[a]

	graphite				*h*-BN			MoS_2		
	LDA	M06-L	XRD[13]	IXS[14]	LDA	M06-L	XRD	LDA	M06-L	XRD[17]
$C_{11} + C_{12}$	1313	1298	1240(40)	1248(52)	1136	1097		299.4	267.6	
C_{13}	−2.8	−3.6	15(5)	0(3)	2.6	0.3		10.9	15.7	
C_{33}	31.3	45.4	36.5(1)	38.7(7)	25.8	40.0		51.9	66.4	
B_0	29.6	42.0	33.8(30)	36.4(11)	24.8	37.2	36.7(5)[15] 20(2)[16]	42.5	51.2	53.4(1)

[a] XRD stands for X-ray diffraction and IXS for inelastic X-ray scattering.

energy. We have also calculated the interlayer cohesive energy, E_l, for graphite. As E_l is small compared to E_c, the reason for the LDA overestimation of the cohesive energy clearly lies in the well-known overbinding of covalent bonds. PBE corrects a large part of the LDA overbinding but overestimates the *c*-axes by almost 40 % with hardly any interlayer binding. The M06-L, on the other hand, gives a good prediction of both the structural properties and the cohesive energy of graphite. M06L underestimates E_l by 11 meV compared to the most recent measurement,[12] whereas LDA underestimates E_l by 27 meV. The M06-L underestimation of E_l could be due to long-range dispersion that is obviously present in the solid but not in the molecular database used to parametrize M06-L. One would expect the LDA overbinding to result in an underestimation of the *a*-axes. However, due the extreme hardness in compressibility along the *a*-axis, as seen from the $C_{11} + C_{12}$ elastic constant in graphite and *h*-BN (Table 2), the underestimation is very small (only about 1 %). The extreme anisotropy of the compressibility in graphite and *h*-BN also leads to a good LDA prediction of the bulk modulus as it is determined almost exclusively by the C_{33} elastic constant (eq 1).

We will now focus on MoS_2, which has a much softer *a*-axis than graphite and *h*-BN. This means that the recently measured[17] bulk modulus will be a linear combination of mainly $C_{11} + C_{12}$ and C_{33}. As seen from Table 2, M06-L gives a bulk modulus in excellent agreement with experiment. Considering the disagreement between the two measurements of the *h*-BN bulk modulus, there might be quite a large uncertainty in the experimental value. However, the good agreement in the bulk modulus is coupled with a very good prediction of the a_0 value, which lends the agreement credibility.

To understand the beneficial effects of including in the MGGA the density gradients and the kinetic energy density terms, we have made a detailed analysis of their distribution in graphite. We will present the results in terms of the two reduced dimensionless quantities

$$p = \frac{|\nabla n|^2}{4(3\pi^2)^{2/3} n^{8/3}} \qquad t^{-1} = \frac{\tau}{\tau^{\mathrm{LDA}}} \tag{2}$$

where n is the density, $\tau = (1/2)\sum f_n |\nabla \psi_n|^2$ the kinetic energy density, and $\tau^{\mathrm{LDA}} = (3/10)(3\pi^2)^{2/3} n^{5/4}$. τ/τ^{LDA} is referred to as t^{-1} to conform with the definition of $t = \tau^{\mathrm{LDA}}/\tau$ that used in the parametrization of the M06-L;[7,18] t^{-1} is related to the $\alpha = (\tau - \tau^{\mathrm{W}})/\tau^{\mathrm{LDA}}$, which we used in our previous paper (τ^{W} is defined in the caption of Figure 2).[19]

In Figure 1, we show values for p and t^{-1} in two different directions in graphite. Inspecting p in Figure 1a, it is seen that the density gradient is zero right between two carbon atoms, irrespective of whether it is a covalent bond or a dispersive interaction. This naturally follows from symmetry considerations and means that a GGA cannot, qualitatively, "see" a difference between a covalent and a dispersive interaction. Turning instead to the kinetic energy term, t^{-1} in Figure 1b, this quantity is seen to adopt two very different values along the two directions, having a minimum in the middle of the covalent bond and a maximum in the middle of the closed-shell interaction. Figure 1c presents a schematic explanation why the kinetic energy term may discriminate between the two types of interaction. Assume an interaction arises from overlap of two atomic orbitals. The resulting bonding and antibonding orbitals are depicted in the middle of Figure 1c. If the interaction is covalent, it means that only the bonding orbital is occupied. This orbital has zero gradient in the middle of the bond, and hence, t^{-1} vanishes. However, if the interaction is dispersive, as for closed shells, then both of the bonding and antibonding orbitals become occupied. Since the antibonding orbital has a large gradient value in the middle of the bond, t^{-1} becomes large.

The scatter plot Figure 2(upper part) illustrates this point. The figure reveals that the only source of small p/large t^{-1}

DOI: 10.1021/jz9002422 | *J. Phys. Chem. Lett.* **2010**, *1*, 515–519

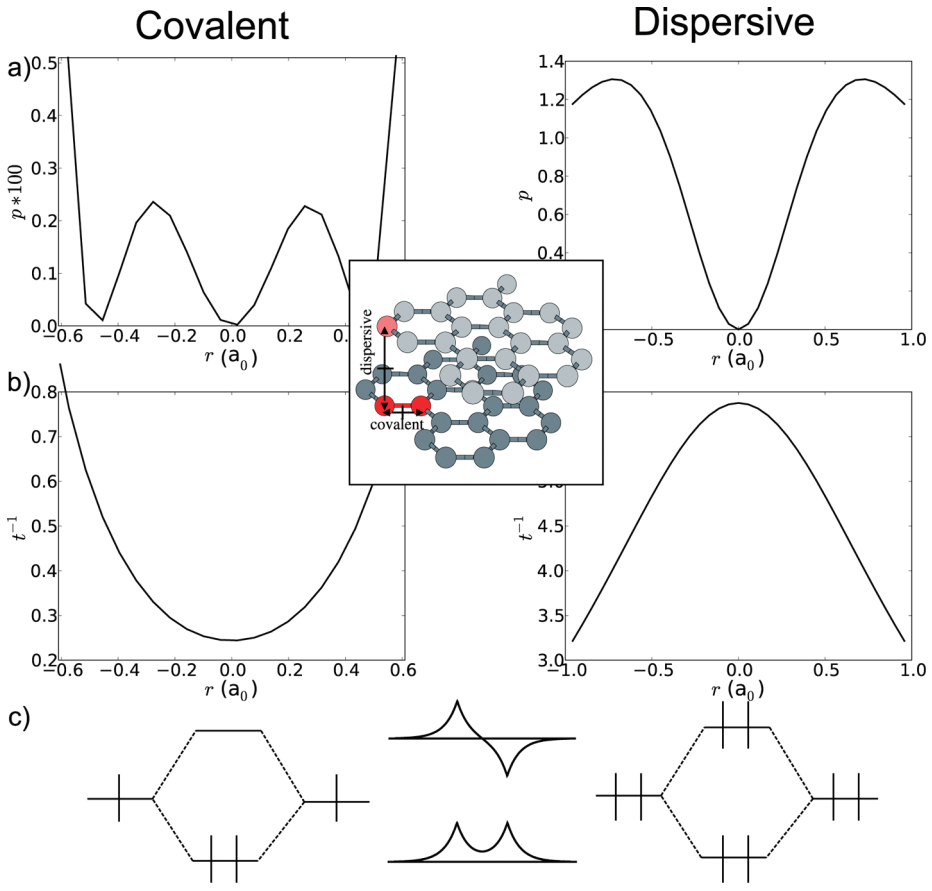

Figure 1. (a,b) The density distribution functions, p and t^{-1}, for graphite at the equilibrium structure. Left part: along the covalent bond. Right part: across from one graphene layer to the next. On the x-axis, $r = 0$ is chosen to be the middle point between two carbon atoms. (c) Schematic drawing of a covalent and dispersive interaction.

combinations is the region midway between the graphene sheets (the yellow points). Thus, regions of closed-shell interactions are fingerprinted in a MGGA. In a GGA, one cannot distinguish between the covalent and the closed-shell areas since the GGA only depends on p and not on t^{-1} (cf. Figure 2 showing red, green, and yellow points when inspecting for small p). The finding that many yellow points in Figure 2 have large p reflects that only every second carbon atom has a neighbor in the vertical direction (see inset in Figure 1). Above and below these atoms, the large p area will extend into the yellow region.

Having established that a MGGA is able to "see" a closed-shell (orbital overlap) interaction by small p/large t^{-1} combinations, we will now look at how the M06-L uses this information. The exchange enhancement of the M06-L (Figure 2) is strongly reduced in the small p/large t^{-1} region of closed-shell overlap. As discussed earlier,[19] p tends to infinity in the tails of the atoms, and consequently, the main effect on the density distribution on expansion of the structure is an increase of volume in which p is large. It is thus clear that GGAs, which enhance the negative exchange energy with increasing p, will prefer expanded structures compared to the LDA (see Table 1), where PBE strongly overestimate the c_0 value. Hence, the lowering of F_x of M06-L in the closed-shell area is necessary to compensate for the gradient enhancement.

Having understood the behavior of the M06-L, we will explain the behavior of two recent functionals and discuss how their failures might be turned to their advantage. First of all, it is known that the TPSS-MGGA[20] does not find any interlayer bonding for graphite at all.[21] This is understandable because the TPSS-MGGA even increases F_x in the region of closed-shell interaction (see the curve for $\alpha = \infty$ at small s in Figure 1 of ref 20). Second, it has been found that the so-called van der Waals density functional (vdW-DF)[22] gives a good prediction of the c-axis (c_0 = 12.6 Å) of MoS_2, whereas the a axis is strongly overestimated (a_0 = 3.23 Å).[6] Compared to graphite, the softer a-axis of MoS_2 is more sensitive to the quality of the functional, and the revealed underbonding can be traced back to the use of revPBE-GGA[23] that is combined with the nonlocal vdW-DF correlation functional.[6] The revPBE was used to avoid van der Waals interactions being included in the exchange but has the side effect that the large gradient enhancement of revPBE leads to a strong underbinding in the covalent layer.[24] The absence of closed-shell bonding in the TPSS combined with its good description of covalent bonding could make it ideally suited for the vdW-DF functional.

In the present Letter, we have tested the MGGA M06-L for three layered solids and shown that it can perform well outside of the database used for its parametrization. At first sight, the behavior of the M06-L is somewhat counterintuitive

DOI: 10.1021/jz9002422 | J. Phys. Chem. Lett. 2010, 1, 515–519

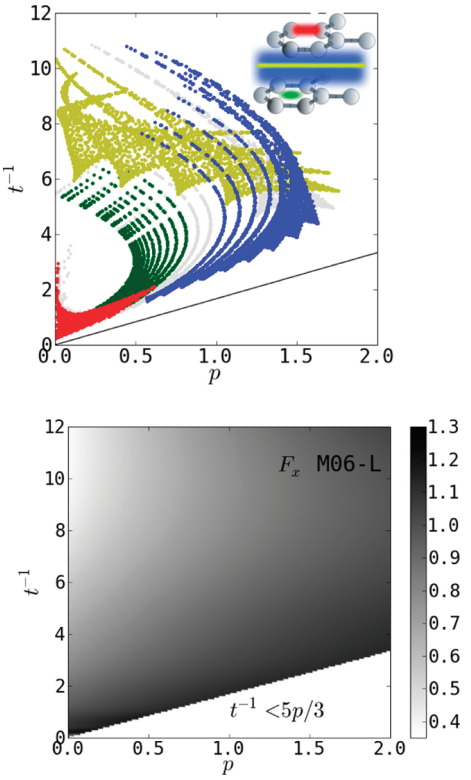

Figure 2. (Top) Scatter plot of the reduced gradients of the pseudodensity in graphite. The (p,t^{-1}) values are color-coded according to their spatial origin. Red, green, blue, and yellow points refer to (p,t^{-1}) values located in the covalent C−C bonds, intralayer hollow regions in the aromatic rings, interlayer regions except the region midway between the graphene sheets, and the region midway between the graphene sheets, respectively. The straight line represents the lower bound $t^{-1} > \tau^W/\tau^{LDA} = 5p/3$, where $\tau^W = |\nabla n|^2/8n$ is the von Weizsäcker kinetic energy density. (Bottom) M06-L exchange enhancement factor defined as $E_x = \int F_x[n,\nabla n,\tau]e_x^{LDA}d^3r$.

for two reasons. First of all, in a one-electron picture, as in Figure 1, the dispersive bond will always be repulsive because of the orthogonalization between the orbitals.[25] However, the exchange-correlation functional should model the many-body effects that give rise to the dispersive forces beyond a one-electron picture. It then might be somewhat surprising that a local functional is able to model interactions which are usually understood in terms of the van der Waals bond. However, also exact exchange is nonlocal and long-range. A local exchange functional should mimic both exchange and long-range correlation when averaged over the entire system.[18] From this point of view, it is just important that a local functional can "see" a closed-shell interaction and respond adequately. The kinetic energy density provides the handle for this, requiring only an orbital overlap, which one would expect at typical van der Waals interaction distances.[26] We do not expect a local functional to correctly handle long-range dispersion, which could explain why M06-L underestimates the interlayer cohesive energy by 11 meV compared to the most recent measurement.

Even if one does not find that a good functional should be based on 25 parameters, the present results show how fitting a flexible functional form can lead to the "discovery" of a desired behavior of a functional. This behavior can inspire the development of new more restricted functionals.

SUPPORTING INFORMATION AVAILABLE Details of the computational procedure. This material is available free of charge via the Internet at http://pubs.acs.org.

AUTHOR INFORMATION

Corresponding Author:

*To whom correspondence should be addressed. E-mail: georg.madsen@rub.de.

ACKNOWLEDGMENT G.M. acknowledges financial support through ThyssenKrupp AG, Bayer MaterialScience AG, Salzgitter Mannesmann Forschung GmbH, Robert Bosch GmbH, Benteler Stahl/Rohr GmbH, Bayer Technology Services GmbH, and the state of North-Rhine Westphalia as well as the European Comission in the framework of the European Regional Development Fund (ERDF).

REFERENCES

(1) Mounet, N.; Marzari, N. First-Principles Determination of the Structural, Vibrational and Thermodynamic Properties of Diamond, Graphite, and Derivatives. *Phys. Rev. B* **2005,** *71*, 205214.
(2) Grimme, S. Semiempirical GGA-Type Density Functional Constructed with a Long-Range Dispersion Correction. *J. Comput. Chem.* **2006,** *27*, 1787.
(3) Grimme, S.; Mück-Lichtenfeld, C.; Antony, J. Noncovalent Interactions between Graphene Sheets and in Multishell (Hyper)Fullerenes. *J. Phys. Chem. C* **2007,** *111*, 11199–11207.
(4) Kerber, T.; Sierka, M.; Sauer, J. Application of Semiempirical Long-Range Dispersion Corrections to Periodic Systems in Density Functional Theory. *J. Comput. Chem.* **2008,** *29*, 2088–2097.
(5) Becke, A. D.; Johnson, E. R. Exchange-Hole Dipole Momemt and the Dispersion Interaction Revisited. *J. Chem. Phys.* **2007,** *127*, 174108.
(6) Dion, M.; Rydberg, H.; Schroder, E.; Langreth, D. C.; Lundqvist, B. I. Van der Waals Density Functional for General Geometries. *Phys. Rev. Lett.* **2004,** *92*, 246401.
(7) Zhao, Y.; Truhlar, D. G. A New Local Density Functional for Main-Group Thermochemistry, Transition Metal Bonding, Thermochemical Kinetics, And Noncovalent Interactions. *J. Chem. Phys.* **2006,** *125*, 194101.
(8) Mortensen, J. J.; Hansen, L. B.; Jacobsen, K. W. Real-Space Grid Implementation of the Projector Augmented Wave Method. *Phys. Rev. B* **2005,** *71*, 035109.
(9) *CRC Handbook of Chemistry and Physics*; Lide, D. R., Ed.; CRC Press: Boca Raton, FL, 2007.
(10) Knittle, E.; Wentzcovitch, R. M.; Jenloz, R.; Cohen, M. L. Experimental and Theoretical Equation of State of Cubic Boron Nitride. *Nature* **1989,** *337*, 349–352.
(11) Benedict, L. X.; Chopra, N. G.; Cohen, M. L.; Zettl, A.; Louie, S. G.; Crespi, V. H. Microscopic Determination of the Interlayer Binding Energy in Graphite. *Chem. Phys. Lett.* **1998,** *286*, 490–496.
(12) Zacharia, R.; Ulbricht, H.; Hertel, T. Interlayer Cohesive Energy of graphite From Thermal Desorption of Polyaromatic Hydrocarbons. *Phys. Rev. B* **2004,** *69*, 155406.

DOI: 10.1021/jz9002422 | *J. Phys. Chem. Lett.* **2010,** *1*, 515–519

(13) Zhao, Y. X.; Spain, I. L. X-ray Diffraction Data for Graphite to 20 GPa. *Phys. Rev. B* **1989,** *40*, 993–997.
(14) Bosak, A.; Krisch, M.; Mohr, M.; Maultzsch, J.; Thomsen, C. Elasticity of Single-Crystalline Graphite: Inelastic X-ray Scattering Study. *Phys. Rev. B* **2007,** *75*, 153408.
(15) Solozhenko, V. L.; Will, G.; Elf, F. Isothermal Compression of Hexagonal Graphite-Like Boron Nitride up to 12 GPa. *Solid State Commun.* **1995,** *96*, 1–3.
(16) Fuchizaki, K.; Nakamichi, T.; Saitoh, H.; Katayama, Y. Equation of State of Hexagonal Boron Nitride. *Solid State Commun.* **2009,** *148*, 390–394.
(17) Aksoy, R.; Ma, Y.; Selvi, E.; Chyu, M. C.; Ertas, A.; White, A. X-ray Diffraction Study of Molybdenum Disulfide to 38.8 GPa. *J. Phys. Chem. Solids* **2006,** *67*, 1914–1917.
(18) Becke, A. D. Simulation od Delocatized Exchange by Local Density Functionals. *J. Chem. Phys.* **2000,** *112*, 4020–4026.
(19) Ferrighi, L.; Hammer, B.; Madsen, G. K. H. 2D-3D Transition for Cationic and Anionic Gold Clusters. A Kinetic Energy Density Functional Study. *J. Am. Chem. Soc.* **2009,** *131*, 10605–10609.
(20) Tao, J.; Perdew, J. P.; Staroverov, V. N.; Scuseria, G. E. Climbing the Density Functional Ladder: Nonempirical Meta-Generalized Gradient Approximation Designed for Molecules and Solids. *Phys. Rev. Lett.* **2003,** *91*, 146401.
(21) (a) Haas, P.; Tran, F.; Blaha, P. Calculation of the Lattice Constant of Solids with Semilocal Functionals. *Phys. Rev. B* **2009,** *79*, 085104. (b) Haas, P.; Tran, F.; Blaha, P. Erratum: Calculation of the Lattice Constant of Solids with Semilocal Functionals. *Phys. Rev. B* **2009,** *79*, 209902(E).
(22) Rydberg, H.; Dion, M.; Jacobson, N.; Schröder, E.; Hyldgaard, P.; Simak, S. I.; Langreth, D. C.; Lundqvist, B. I. Van der Waals Density Functional for Layered Structures. *Phys. Rev. Lett.* **2003,** *91*, 126402.
(23) Zhang, Y.; Yang, W. Comment on "Generalized Gradient Approximation Made Simple". *Phys. Rev. Lett.* **1998,** *80*, 890–890.
(24) Madsen, G. K. H. Functional Form of the Generalized Gradient Approximation for Exchange: The PBEα Functional. *Phys. Rev. B* **2007,** *75*, 195108.
(25) Hammer, B.; Nørskov, J. K. Why gold is the Noblest of All the Metals. *Nature* **1995,** *376*, 238–240.
(26) Mantina, M.; Chamberlin, A. C.; Valero, R.; Cramer, C. J.; Truhlar, D. G. Consistent van der Waals Radii for the Whole Main Group. *J. Phys. Chem. A* **2009,** *113*, 5806–5812.

DOI: 10.1021/jz9002422 | *J. Phys. Chem. Lett.* **2010,** *1*, 515–519